Chinese Chemical Letters 36 (2025) 109848

Contents lists available at ScienceDirect

Chinese Chemical Letters

journal homepage: www.elsevier.com/locate/cclet

Logically integrating exo/endogenous gated DNA trackers for precise microRNA imaging *via* synergistic manipulation

Fanghua Zhang[a,1], Yuyan Li[a,1], Hongyan Zhang[a], Wendong Liu[a], Zhe Hao[a], Mingzheng Shao[a], Ruizhong Zhang[a], Xiyan Li[b], Libing Zhang[a,*]

[a] *Tianjin Key Laboratory of Molecular Optoelectronic Sciences, Department of Chemistry, Tianjin University, Tianjin 300072, China*
[b] *Institute of Photoelectronic Thin Film Devices and Technology, Solar Energy Conversion Center, Key Laboratory of Photoelectronic Thin Film Devices and Technology of Tianjin, Engineering Research Center of Thin Film Photoelectronic Technology of Ministry of Education, Nankai University, Tianjin 300350, China*

ARTICLE INFO

Article history:
Received 22 November 2023
Revised 12 March 2024
Accepted 1 April 2024
Available online 2 April 2024

Keywords:
Stimuli-responsive
DNA tracker
Synergistic manipulation
Spatiotemporal imaging
microRNAs

ABSTRACT

Nanomaterials provide an ideal platform for biomolecular display due to their dimensions approach the molecular scale, facilitating binding behavior akin to that observed in solution-based processes. DNA nanoprobes hold great promise as miniature detectives capable of detecting miRNAs within cells. However, current nanoprobes face a challenge in achieving the required precision for accurate miRNA detection, particularly within the intricate confines of the cellular microenvironment, due to interference with biological autofluorescence, off-target effects, and a lack of spatiotemporal control. Here, we have designed a dual-stimuli responsive DNA tracker, synergistically utilizing specific intracellular cues and external triggers, which enables spatiotemporal-controlled and precise detection and imaging of miRNAs "on demand". The tracker, which combines zeolitic imidazolate framework-67 (ZIF-67) and unique hairpin DNA structures, effectively anchored onto the ZIF-67 through electrostatic interactions, remains in a dormant state until activated by abundant cellular ATP, resulting in the release of the hairpin structures that include a PC linker incorporated into the loop region. Subsequent irradiation triggers specific recognition of the target miRNA. The newly developed HP-PC-BT@ZIF-67 tracker demonstrates precise spatiotemporal miRNA detection and exhibits excellent biocompatibility, enabling specific miRNA recognition "on demand" within cancer cells. This research presents a reliable miRNA imaging platform in the intricate cellular environment, opening up the possibilities for precise biomedical analysis and disease diagnosis.

MicroRNAs (miRNAs) are a class of small non-coding RNAs, typically consisting of approximately 22 nucleotides [1], and they have been demonstrated to be involved in a variety of cell cycle activities as a highly conserved regulatory factor [2,3]. However, the aberrant expression of miRNAs is closely associated with human diseases, such as lipid metabolism disorders and the onset, progression, and metastasis of cancer, along with resistance to therapy [4–6]. There is growing evidence indicating that miRNAs have emerged as promising biomarkers for cancer diagnosis and prognosis [7–9]. The intricate cellular environment poses a significant challenge for monitoring and tracking miRNAs. Conventional intracellular miRNA detection faces a significant limitation, with the activation of "always active" systems occurring upon binding to extracellular targets before reaching the intended intracellular location, leading to compromised detection accuracy and a diminished signal-to-noise ratio [10–12].

To overcome these challenges, responsive probes designed to react to specific stimuli have been developed for miRNA analysis [13–17]. Among these, the light-activated probe, by controlling the imaging process at desired temporal and spatial dimensions [18–20], not only significantly alleviates the problems mentioned above but also enables "on-demand" miRNA detection in the temporal dimension [10,21,22]. Nonetheless, the existing strategies still suffered from a limitation associated with uncontrollable activation, leading to noticeably increased intercellular background signal particularly when the desired target miRNAs have leaked into the surrounding interstitial fluid from cell cytoplasm [23]. In this context, endogenous stimulus-responsive probes, such as adenosine 5′-triphosphate (ATP), glutathione (GSH), and enzymes, have been explored for miRNA imaging [24–27]. These probes have mit-

* Corresponding author.
E-mail address: libing.zhang@tju.edu.cn (L. Zhang).
[1] These authors contributed equally to this work.

https://doi.org/10.1016/j.cclet.2024.109848
1001-8417/

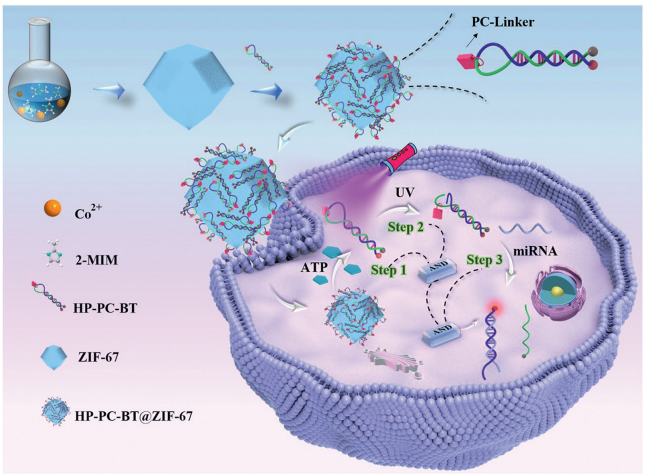

Scheme 1. Synthesis of a tracker (HP-PC-BT@ZIF-67), and intracellular miRNA-21 in living cells with precise imaging.

igated background signals between the cytoplasm and interstitium to some extent [28–30], thereby improving the signal-to-noise ratio [31–33]. However, the challenge remains in achieving precise imaging in both spatial and temporal dimensions [34,35].

Herein, we developed a dual-stimuli responsive DNA tracker for spatially and temporally controlled, on-demand, and precise imaging of intracellular miRNAs (Scheme 1). This tracker combined hairpin probes with zeolitic imidazolate framework-67 (ZIF-67) through electronic interaction, denoted as HP-PC-BT@ZIF-67, which responds to specific intracellular cues and external triggers. To avoid false positive signals in the presence of miRNA at non-target sites, the hairpin probe was designed to conclude with four base pairs (CGCG-CGCG), forming a stable beacon structure. At the ends of this structure, modifications were incorporated, featuring a fluorophore (TAMRA) and a quenching group (BHQ2), with a PC-linker strategically introduced in the loop of the hairpin probe. This unique design ensures that the fluorescence signal remains at a low background level in its initial state. Upon entering cells, the tracker releases the hairpin probe in response to high ATP concentration in tumor cells. UV radiation cleaves the PC-linker, triggering fluorescence signal activation for spatiotemporally controlled miRNA imaging. The system successfully operates a combinational logic circuit (AND) for cascade imaging in living cells, representing a novel dual-activation cascading gate control strategy for precise miRNA imaging. The main features of our unique system include: (i) a significant improvement in the signal-to-noise ratio, thereby greatly enhancing detection precision, (ii) the accomplishment of spatiotemporally controllable "on-demand" imaging through photo-stimulation, and (iii) the effective delivery of hairpin probes through ingenious design while simultaneously implementing an ATP gate control strategy. The successful amalgamation of these distinctive features provides robust support for precise miRNA imaging.

For the preparation of the novel tracker, ZIF-67 MOFs were first synthesized according to the reported method in previously published work [36]. Scanning electron microscopy (SEM) analysis (Fig. 1A) and transmission electron microscopy (TEM) images (Fig. S1A in Supporting information) revealed that the resulting ZIF-67 MOFs displayed the distinctive rhombic dodecahedral structure with an average particle size of approximately 200 nm. Energy-dispersive spectroscopy (EDS) mapping shows that ZIF-67 contains C, N, O, and Co elements (Fig. S1B in Supporting information), where the Co element is from $Co(NO_3)_2$ and the C, N, and O elements are from the 2-methylimidazole (2-MIM) ligand. Subsequently, the crystal structures of the MOFs were analyzed using an

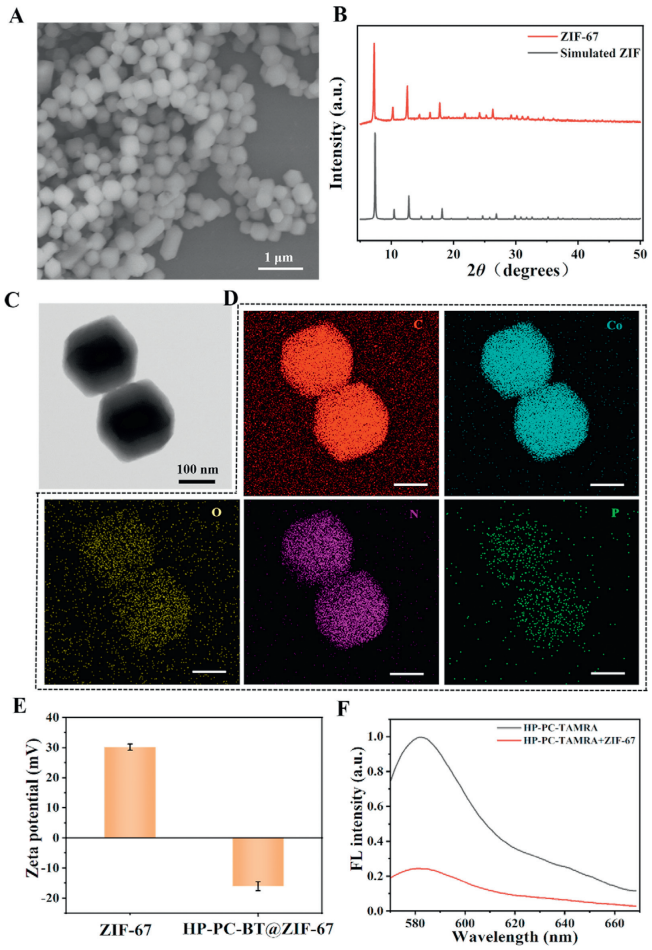

Fig. 1. Characterizations of ZIF-67 and HP-PC-BT@ZIF-67. (A) SEM image and (B) XRD spectra of ZIF-67. (C) TEM image and (D) EDS mapping images of C, N, O, Co, and P for HP-PC-BT@ZIF-67. Scale bars: 100 μm. (E) Zeta potential analysis and (F) fluorescence spectra of HP-PC-TAMRA and HP-PC-TAMRA@ZIF-67.

X-ray diffractometer (XRD) (Fig. 1B). The results show that the pronounced diffraction peaks of the synthesized ZIF-67 are consistent with the simulated diagram, affirming the excellent crystallinity of the MOFs. In addition, Fourier transform infrared spectra disclosed distinct peaks: those at 1582 cm^{-1} represented C=N stretching vibrations, while those at 1418, 1140, and 990 cm^{-1} corresponded to C–N stretching vibrations. Additionally, the peaks at 1303 cm^{-1} indicated N stretching vibrations in the amino group, and those at 426 cm^{-1} denoted Co-N stretching vibrations (Fig. S2A in Supporting information). Notably, the peak at 1303 cm^{-1} signified the stretching vibration of N in the amino group, and the peak at 426 cm^{-1} indicated the stretching vibration of Co-N. The elemental composition of the MOFs was evaluated using X-ray photoelectron spectroscopy (XPS) (Fig. S2B in Supporting information). The results indicate the presence of C, N, O, and Co elements is consistent with the compositions used in the ZIF-67 preparation process and agreement with the EDS results. The above characterization strongly supports the successful synthesis of ZIF-67.

Subsequently, the tracker HP-PC-BT@ZIF-67 was obtained by incubating a hairpin DNA probe (HP-PC-BT) with ZIF-67. TEM images (Fig. 1C) revealed that the morphology of the MOFs remained unchanged after DNA functionalization with an average particle size of approximately 200 nm. Moreover, EDS mapping images exhibited a uniform distribution of C, N, O, Zr, and P elements in the obtained trackers (Fig. 1D). The presence of P element indicated the successful loading of hairpin DNA probes. The ZIF-67 surface

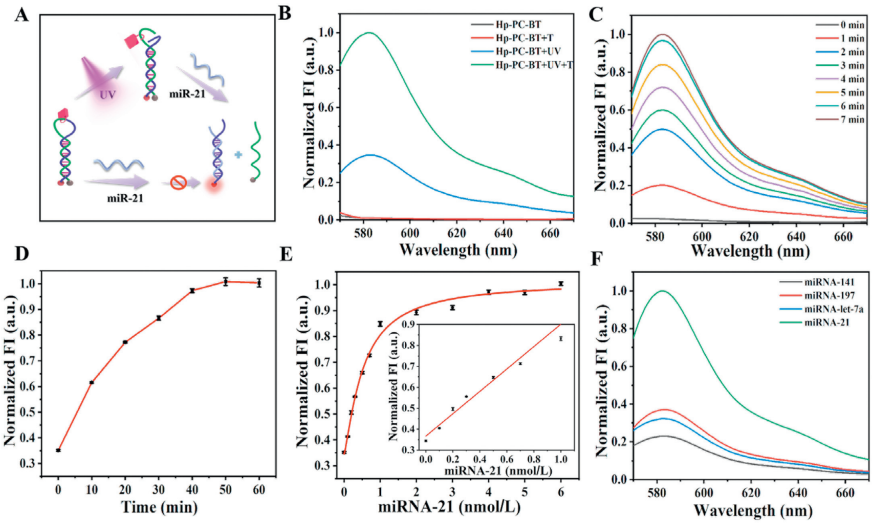

Fig. 2. Investigation of the feasibility of the UV-activated hairpin probe. (A) Schematic demonstration of the UV-activated (365 nm, 2.5 mW/cm^2) hairpin probe and miRNA recognition. (B) Fluorescent light of feasibility experiment of UV-activated hairpin probe under UV irradiation. (C) Fluorescence spectra of HP-PC-BT probes triggered by miRNA-21 under UV irradiation at different times. (D) Time-dependent modulation of HP-PC-BT fluorescence intensity induced by miRNA-21 following UV activation. (E) The linear relationship between fluorescence intensity and miRNA-21 concentration. (F) Fluorescence spectra of HP-PC-BT triggered by different miRNAs after UV irradiation.

held a positive charge in the solution, enabling it to adsorb negatively charged hairpin probes [36]. The analysis of zeta potential revealed a significant potential shift from 30 mV to −16 mV after loading DNA probes, further affirming the successful loading of the hairpin probe (Fig. 1E). Additionally, fluorescence spectra demonstrated a significant quenching of fluorescence in HP-PC-TAMRA upon the addition of HP-PC-TAMRA to the ZIF-67 solution (Fig. 1F), providing clear evidence of the successful adsorption of the hairpin probe onto the ZIF-67 surface. The above findings substantiate the successful preparation of the tracker.

To elucidate the principle of the present sensing system, we demonstrated the working process of the UV-activated hairpin probes (Fig. 2A) and conducted a feasibility analysis of its operation. For precise UV control, this probe was designed with a PC linker incorporated into the loop structure, and also modified with a fluorophore (TAMRA) and a quenching component (BHQ2) at each end of the hairpin probe, facilitating *in vitro* detection of miRNAs under UV irradiation. The hairpin probe, denoted as HP-PC-BT, exhibited a specific configuration that led to Förster resonance energy transfer (FRET) between TAMRA and BHQ2 due to their proximity, resulting in fluorescence quenching in its initial state. However, upon exposure to UV irradiation (2.5 mW/cm^2, 5 min), the fluorescence signal of the hairpin probe was substantially restored in the presence of miRNA-21 within the target cells. Importantly, this response was not observed in control experiments without miRNA-21 or UV irradiation. These results affirm the stability and selectivity of the hairpin probe for miRNA-21 detection, with UV light serving as the trigger (Fig. 2B). Furthermore, we investigated the effect of UV irradiation duration on the hairpin probe and observed that the maximum fluorescence response could be achieved within 7 min (Fig. 2C and Fig. S3A in Supporting information). Additionally, we examined the response time targeting miRNA-21 (Fig. 2D) and found that the fluorescence signal of HP-PC-BT reached its peak within 1 h. Moreover, we recorded the fluorescence spectra across varying concentrations of miRNA-21 to monitor changes in fluorescence intensity (Fig. S3 in Supporting information). Notably, as the concentration of miRNA-21 increased, there was a proportional rise in fluorescence intensity. Within the concentration range of 0.1-1 nmol/L, a linear relationship was obtained between fluorescence intensity and miRNA-21 concentration (Fig. 2E), and the detection limit was calculated to be 0.023 nmol/L. The result indicates the light-activated tracker system can be applied to detect miRNA-21 *in vitro* with sensitivity. For the selectivity, in comparison to the target miRNA-21, the fluorescence signal changes induced by other microRNAs were negligible (Fig. 2F), indicating the excellent specificity of the probe. Overall, our findings demonstrate the potential of the hairpin probe in enabling spatiotemporal control of miRNA detection.

For the constructed HP-PC-BT@ZIF-67 probe, since MOF can quench the fluorescence of dye-labeled DNA by a process called photoelectron transfer (PET) [35], we investigated the fluorescence properties of hairpin probes on MOF using HP-PC-TAMRA (unmodified with a quenching agent). As shown in Fig. S4 (Supporting information), the fluorescence intensity of HP-PC-TAMRA gradually decreased with increasing concentrations of ZIF-67, and the loading efficiency was calculated to be approximately 90.9%, indicating a high nucleic acid loading capacity. Additionally, ZIF-67 exhibited rapid DNA adsorption kinetics, with HP-PC-TAMRA being adsorbed onto the ZIF-67 surface within 5 min (Fig. S5 in Supporting information). The tracker also demonstrated excellent storage stability, with no noticeable DNA leakage even after incubation in water for 24 h (Fig. S6 in Supporting information). ZIF-67 demonstrated strong interactions with the DNA through electrostatic interactions coupling with π-π stacking and hydrogen bonding, enhancing its potential as a valuable component in biosensors [37]. Furthermore, it also exhibited a high affinity and specificity for ATP adsorption, a feature that was leveraged to achieve the desorption of hairpin probes through competitive ATP release [36,38]. To achieve precise spatiotemporal control over ultraviolet light, we initially explored the feasibility of desorbing hairpin probes from the surface of ZIF-67 (Fig. 3A). Recognizing that the concentration of ATP in tumor cells could reach up to approximately 1–10 mmol/L, surpassing the ATP levels in normal cells by four orders of magnitude [6], we elevated the added ATP amount from 0 to 10 mmol/L to mimic the high ATP levels observed in tumor cells. We measured the resulting fluorescence intensity of the released HP-PC-TAMRA, and as anticipated, the fluorescence intensity of HP-PC-TAMRA@ZIF-67 increased proportionally with the rising ATP content (Fig. 3B and Fig. S7 in Supporting information), demonstrating the precision of HP-PC-TAMRA@ZIF-67 in responding to *in situ* cellular ATP levels. Moreover, the fluorescence enhancement kinetics of ZIF-67 were remarkably rapid, with over 50% of the adsorbed DNA strands being desorbed by ATP within just 10 min (Fig. 3C). Subsequently, the results of an ATP response specificity experiment indicated

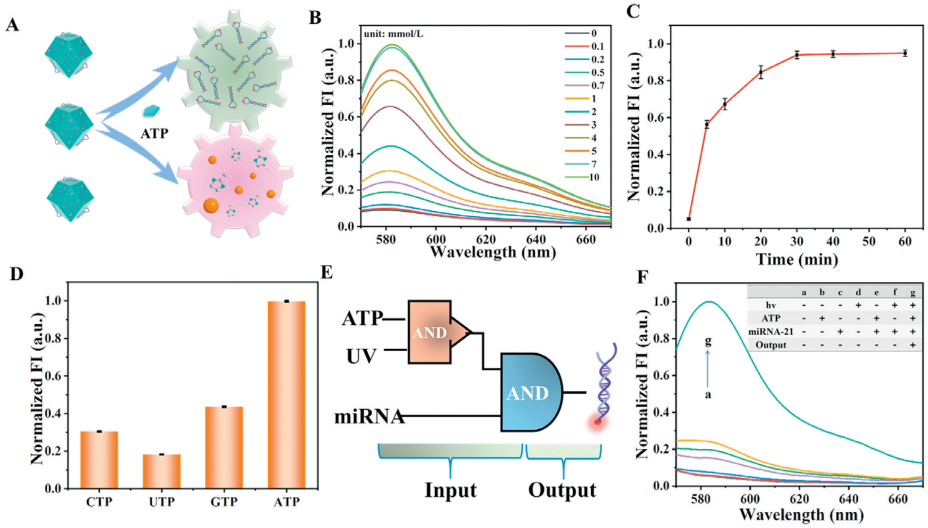

Fig. 3. The ability of HP-PC-TAMRA to release from the surface of ZIF-67 and the feasibility of *in vitro* detection of miRNA by HP-PC-BT@ZIF-67. (A) Schematic demonstration of the ATP response of the tracker and the release of the hairpin probe. (B) Fluorescence spectra of HP-PC-TAMRA@ZIF-67 at different concentrations of ATP. (C) The fluorescence intensity of HP-PC-TAMRA@ZIF-67 changed with time after adding 5 mmol/L ATP. (D) Selectivity of HP-PC-TAMRA@ZIF-67 toward ATP. (E) Schematic demonstration of the cascade process for detecting miRNA. (F) Fluorescence spectra of HP-PC-BT@ZIF-67 under different conditions (a, HEPES; b, 5 mmol/L ATP; c, 5 nmol/L miRNA-21; d, UV irradiation; e, 5 nmol/L miRNA-21 and 5 mmol/L ATP; f, UV irradiation and 5 nmol/L miRNA-21; g, UV irradiation, 5 nmol/L miRNA-21 and 5 mmol/L ATP).

that no noticeable fluorescence signal was observed in the presence of other nucleosides such as GTP, UTP, and CTP, underscoring the excellent selectivity of ZIF-67 for ATP. To elucidate this phenomenon, we introduced a variety of molecules as competitive agents for desorbing DNA, including CTP, UTP, GTP, and ATP. Notably, only ATP induced a pronounced fluorescence signal for the HP-PC-TAMRA@ZIF-67 sample (Fig. 3D). In contrast, negligible responses were observed for other nucleotide triphosphates such as GTP, CTP, and UTP. The desorption is attributed to competitive ATP adsorption. Consequently, ZIF-67 appears to possess the dual capability of recognizing both the nucleobase and triphosphate of ATP [36]. This implies a robust interaction between the phosphate backbone and adenine with ZIF-67, with each interaction being notably strong. Successful desorption of DNA is achieved only when ATP competes for both of these interactions. This underscores the potential of the system to serve as a highly sensitive and selective biosensor for ATP detection.

Furthermore, we conducted the light activation and ATP response tests using a gated logic assembly strategy to assess the feasibility of the tracker for miRNA-21 detection, as depicted in Fig. 3E. When exposed to a low concentration of ATP within a 60-min timeframe, HP-PC-BT remained immobilized on ZIF-67, resulting in no significant fluorescence signal after UV light irradiation, even upon the addition of the target miRNA-21. Conversely, when a high concentration of ATP was introduced, HP-PC-BT was released from ZIF-67, and the fluorescence intensity of the tracker gradually increased with the rising ATP concentration after UV light irradiation (Fig. S8 in Supporting information). We further investigated the response of the tracker to miRNA-21 under various conditions. In a HEPES solution, the tracker exhibited the lowest fluorescence signal (Fig. 3F, line a). Subsequently, upon the separate addition of ATP (Fig. 3F, line b) and miRNA-21 (Fig. 3F, line c), no significant change in the fluorescence signal of the tracker was observed. Even after UV light exposure, the tracker remained non-fluorescent due to the non-release of HP-PC-BT from the ZIF-67 surface and the absence of miRNA-21 to initiate the reaction (Fig. 3F, line d). Similarly, in the presence of both ATP and miRNA-21, there was no observable fluorescence change for the tracker (Fig. 3F, line e). When the tracker was subjected to UV light irradiation followed by the introduction of target miRNA-21, there was no significant fluorescence signal enhancement due to the continuous attachment of the activation probe to the ZIF-67 surface, preventing hybridization with the target miRNA-21 (Fig. 3F, line f). However, significant fluorescence signal enhancement (Fig. 3F, line g) was observed when HP-PC-BT@ZIF-67 was supplemented with ATP, followed by UV light activation and co-incubation with miRNA-21. From the above results, we conclude that the tracker can be used for miRNA-21 detection under the synergistic effect of photoactivation and ATP response. Importantly, low concentrations of ATP in normal cells do not restore the fluorescent signal (Fig. S8 in Supporting information), thus enhancing the tumor-specificity of miRNA-21 detection.

To be considered suitable for biological applications, the designed tracker must exhibit minimal cellular toxicity. Consequently, we conducted MTT assays to assess the cytotoxicity of the tracker, as the biocompatibility of such probes is critical for cell imaging analysis. After 24 h of incubation with the tracker at a concentration of 1 mg/mL, HeLa cell viability remained over 86% (Fig. 4A), indicating the low cytotoxicity of the tracker. Furthermore, we investigated the impact of UV light irradiation on cell viability, and the results revealed that more than 89% of HeLa cells remained viable even after 7 min of UV light exposure (Fig. 4B). And the impact on normal cells (HEK293T) can be considered negligible (Fig. S10 in Supporting information). These findings collectively demonstrate that the tracker can be safely used in subsequent cell imaging experiments, with minimal cytotoxicity, and that UV light exposure does not significantly harm cells in the absence of the tracker. Additionally, we explored the internalization behavior of cells concerning the tracker at different time points. The tracker was co-cultured with cells for durations of 2, 4, 6, and 8 h Confocal laser scanning microscopy (CLSM) analysis revealed that the tracker was widely distributed within the cytoplasm, with the fluorescence intensity reaching its peak at 6 h (Figs. 4C and D). Furthermore, we investigated whether the hairpin probe could enter the cell alone by co-incubating the hairpin probe and the tracker with the cell for 6 h, respectively. When the hairpin probe was incubated with the cells, it showed limited cellular uptake and fluorescence intensity. In contrast, the tracker designed in this study was able to efficiently enter the cell and was massively distributed in the cytoplasm, leading to a significantly increased fluorescence intensity in HeLa cells compared to untreated cells (Fig. 4E and Fig. S11 in Supporting information). This further underscores the efficacy of the tracker for cellular imaging applications.

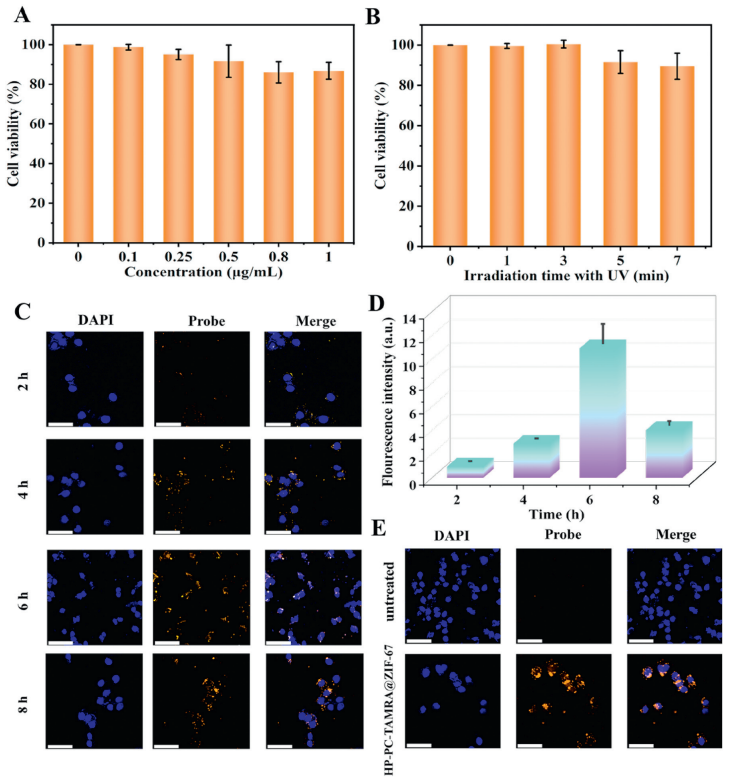

Fig. 4. Cell viability and CLSM images of HeLa cells. (A) Cell viability of HeLa cells incubated with different concentrations of HP-PC-TAMRA@ZIF-67 for 24 h and (B) exposed to different light times (365 nm, 2.5 mW/cm^2), data are represented as means ± SD ($n = 3$). (C) Time-dependent *in situ* confocal imaging of HeLa cells incubated with HP-PC-TAMRA@ZIF-6. Scale bar: 50 μm. (D) Quantification of the CLSM images data in (C), data are represented as means ± SD ($n = 3$). (E) HeLa cells were processed using HP-PC-TAMRA@ZIF-67. Scale bar: 50 μm.

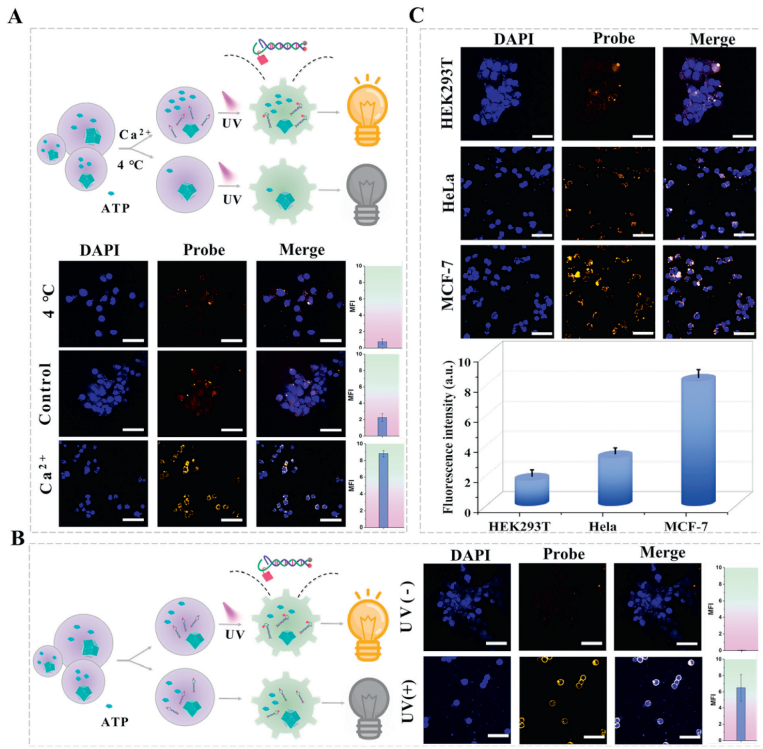

Fig. 5. CLSM image of tracker under different conditions. (A) CLSM imaging of HeLa cells treated with various formulations, with corresponding MFI histogram analysis on the right. Scale bar: 50 μm. (B) CLSM imaging of HeLa cells treated under UV (365 nm, 2.5 mW/cm^2) and non-UV irradiation. Scale bar: 50 μm. (C) The image of HEK293T, HeLa, and MCF-7 cells treated after UV light activation. Scale bar: 50 μm. Data are represented as mean ± SD ($n = 3$).

Subsequently, we sought to assess the capability of the tracker for spatiotemporal controlled imaging of miRNAs within living cells. To achieve this, we pretreated HeLa cells with either Ca^{2+} or subjected them to a 4 °C incubation to enhance or reduce intracellular ATP production [39,40]. Compared to untreated cells, the Ca^{2+}-pretreated cells exhibited a substantially higher fluorescence output, while the cells subjected to low-temperature (4 °C) incubation displayed negligible fluorescence intensity (Fig. 5A). Additionally, a significantly elevated fluorescence output was observed upon UV light stimulation when the tracker was co-cultured with HeLa cells (Fig. 5B). These results emphasize the indispensable roles of high ATP concentration and UV light in the miRNA-21 tracking process within the tracker. Next, we utilized the novel tracker to assess miRNA-21 expression levels in three distinct cellular contexts characterized by varying miRNA-21 abundances. We tested the tracker on three different cell lines (including MCF-7, HeLa, and HEK293T cells). Notably, the strongest fluorescence signal post-UV activation was observed in MCF-7 cells, followed by a slightly weaker signal in HeLa cells, and a negligible signal in HEK293T cells (Fig. 5C). This disparity can be attributed to the significantly higher ATP content and miRNA-21 expression levels in MCF-7 cells. The synergistic interplay between photoactivation and ATP response thus generated a robust fluorescent signal for miRNA detection. Overall, the designed dual-stimulus responsive tracker demonstrates precise imaging and selectivity for detecting intracellular miRNA-21. It holds promise in distinguishing cancer cells from normal cells by leveraging differences in miRNA-21 expression levels and ATP concentrations.

In summary, we have developed an exo/endogenous gated tracker for the precise imaging of cancer-specific miRNAs with enhanced spatial accuracy and signal-to-noise ratio. Efficient loading of hairpin probes is achieved through electrostatic interactions between ZIF-67 and DNA phosphate backbones. The excellent biocompatibility of ZIF-67 also enhances the cellular uptake efficiency of DNA nanoprobes. Leveraging the unique affinity of ZIF-67 for ATP, we designed a tracker with tumor specificity. Furthermore, the presence of the PC linker enabled the tracker to achieve spatiotemporally controlled imaging of miRNAs, overcoming the drawback of previous DNA nanoprobes prone to uncontrolled activation during intracellular delivery, resulting in inaccurate miRNA detection. In conclusion, our research introduces a pioneering method for achieving precise spatiotemporal-controlled imaging of miRNA-21 through UV light activation and endogenous ATP response, offering promise for early cancer diagnosis and the exploration of various biomarkers.

Declaration of competing interest

The authors declare that they have no known competing financial interests or personal relationships that could have appeared to influence the work reported in this paper.

CRediT authorship contribution statement

Fanghua Zhang: Investigation, Methodology, Validation, Writing – original draft, Writing – review & editing. **Yuyan Li:** Investigation, Methodology, Validation. **Hongyan Zhang:** Formal analysis, Investigation. **Wendong Liu:** Investigation. **Zhe Hao:** Conceptualization. **Mingzheng Shao:** Formal analysis, Investigation. **Ruizhong Zhang:** Conceptualization, Resources, Writing – review & editing. **Xiyan Li:** Conceptualization, Resources, Writing – review & editing. **Libing Zhang:** Conceptualization, Funding acquisition, Resources, Supervision, Writing – review & editing.

Acknowledgments

This work was supported by the National Natural Science Foundation of China (Nos. 21904095, 22004089), Peiyang Talents Project of Tianjin University, Young Thousand Talented Program, and Program of Tianjin Science and Technology Major Project and Engineering (No. 19ZXYXSY00090).

Supplementary materials

Supplementary material associated with this article can be found, in the online version, at doi:10.1016/j.cclet.2024.109848.

References

[1] X. Meng, K. Zhang, F. Yang, et al., Anal. Chem. 92 (2020) 8333–8339.
[2] S. Asaga, C. Kuo, T. Nguyen, et al., Clin. Chem. 57 (2011) 84–91.
[3] X. Sun, H. Wang, Y. Jian, et al., Biosens. Bioelectron. 105 (2018) 218–225.
[4] E.J. Lee, Y. Gusev, J. Jiang, et al., Int. J. Cancer. 120 (2007) 1046–1054.
[5] L. Gorgani, M. Mohammadi, G.N. Darzi, J.B. Raoof, Sensor. Actuat. B: Chem. 378 (2023) 133194.
[6] X. Li, F. Yang, S. Li, R. Yuan, Y. Xiang, Anal. Chem. 94 (2022) 9927–9933.
[7] J.Y. Hwang, S.T. Kim, J. Kwon, et al., ACS Sens. 3 (2018) 2651–2659.
[8] B. Li, Y. Liu, Y. Liu, et al., ACS Nano 14 (2020) 8116–8125.
[9] R. Liu, S. Zhang, T.T. Zheng, et al., ACS Nano 14 (2020) 9572–9584.
[10] X.Y. Sun, X. Wei, K.X. Liu, et al., Sensor. Actuat. B: Chem. 396 (2023) 134533.
[11] M. Ye, Y. Kong, C. Zhang, et al., ACS Nano 15 (2021) 14253–14262.
[12] R. Deng, K. Zhang, J. Li, Acc. Chem. Res. 50 (2017) 1059–1068.
[13] J. Zhan, Z. Liu, R. Liu, et al., Anal. Chem. 94 (2022) 16622–16631.
[14] X. Zhao, L. Zhang, W. Gao, et al., ACS Appl. Mater. Interfaces 12 (2020) 35958–35966.
[15] Y. Shen, Z. Li, G. Wang, N. Ma, ACS Sens. 3 (2018) 494–503.
[16] C.C. Li, J. Hu, X. Luo, J. Hu, C.Y. Zhang, Anal. Chem. 93 (2021) 14568–14576.
[17] X. He, T. Zeng, Z. Li, et al., Angew. Chem. Int. Ed. 55 (2016) 3073–3076.
[18] N. Melnychuk, S. Egloff, A. Runser, A. Reisch, A.S. Klymchenko, Angew. Chem. Int. Ed. 59 (2020) 6811–6818.
[19] L. Jiang, H.Y. Chen, C.H. He, et al., Anal. Chem. 95 (2023) 3507–3515.
[20] W. Wang, N.S.R. Satyavolu, Z. Wu, et al., Angew. Chem. Int. Ed. 56 (2017) 6798–6802.
[21] Y. Wen, W.Y. Liu, J.H. Wang, et al., Anal. Chem. 95 (2023) 12152–12160.
[22] J.W. He, X.M. Sun, Y.L. Chen, et al., Sensor. Actuat. B: Chem. 384 (2023) 133660.
[23] Q. Liu, Y. Huang, Z. Li, et al., Angew. Chem. Int. Ed. 61 (2022) e202214230.
[24] J. Wang, J. Li, Y. Chen, et al., Nano Lett. 22 (2022) 8216–8223.
[25] T. Zhao, Y. Gao, J. Wang, et al., Anal. Chem. 93 (2021) 12329–12336.
[26] J. Zhao, H. Chu, Y. Zhao, Y. Lu, L. Li, J. Am. Chem. Soc. 141 (2019) 7056–7062.
[27] J. Zhao, J. Gao, W. Xue, et al., J. Am. Chem. Soc. 140 (2018) 578–581.
[28] Y. Feng, Q. Liu, X. Zhao, et al., Anal. Chem. 94 (2022) 2934–2941.
[29] X. Liu, X. Wang, S. Ye, et al., ACS Appl. Mater. Interfaces 13 (2021) 27825–27835.
[30] Y. Li, F. Zhang, W. Liu, et al., Chem. Commun. 59 (2023) 5431–5434.
[31] X. Meng, H. Wang, M. Yang, et al., Anal. Chem. 93 (2021) 1693–1701.
[32] N. Yan, L. Lin, C. Xu, et al., Small 15 (2019) 1903016.
[33] Y. Zhou, L. Zou, G. Li, et al., Anal. Chem. 93 (2021) 13960–13966.
[34] D.X. Wang, J. Wang, Y.X. Cui, et al., Anal. Chem. 91 (2019) 13165–13173.
[35] L. Feng, M. Liu, H. Liu, et al., ACS Appl. Mater. Interfaces 10 (2018) 23647–23656.
[36] Z. Wang, X. Zhou, Y. Li, et al., Anal. Chem. 93 (2021) 7707–7713.
[37] X. Zhu, H. Zheng, X. Wei, et al., Chem. Commun. 49 (2013) 1276–1278.
[38] Y. Lu, J. Li, Y. Liu, et al., Microchimica Acta 190 (2023) 71.
[39] E.J. Griffiths, G.A. Rutter, BBA Bioenergetics 1787 (2009) 1324–1333.
[40] Q. Wu, L. Yang, L. Xie, et al., Small 18 (2022) 2200983.